Fermilab

FERMILAB-PUB-13-159-APC
May 2013

RADIATION STUDIES FOR THE MU2E EXPERIMENT: A REVIEW*

V.S. Pronskikh

Fermi National Accelerator Laboratory, Batavia IL 60510-5011, USA

Abstract

The Mu2e experiment being designed at Fermilab will be searching for a rare event -- conversion of muon into electron the field of a nucleus without emission of neutrinos -- observation of which would provide unambiguous evidence for physics beyond the Standard Model, making use of an 8 GeV 8 kW proton beam. As an experiment to be performed at the Fermilab's Intensity Frontier, taking advantage of high-intensity proton beams, Mu2e experimental setup will be residing in a harsh radiation environment, created by secondary particle fluxes.

Radiation quantities in different parts of the Mu2e apparatus, such as neutron flux, peak power density, DPA, absorbed dose, dynamicheat load simulated using the MARS15 code are reviewed in this work. Radiation levels and requirements for Heat and Radiation Shield (HRS), Transport Solenoid, residual dose and decay heat from the Mu2e target, beam dump design, rates in Cosmic Ray Veto counters as well as stopping target monitor are considered. Airflow, surface, and ground water activation are estimated. Recent developments in the MARS15 DPA model applied in this work are described, its consequences are discussed.

*Work supported by Fermi Research Alliance, LLC under contract No. DE-AC02-07CH11359 with the U.S. Department of Energy.
§ Corresponding author. Email: vspron@fnal.gov

Modern Physics Letters A

RADIATION STUDIES FOR THE MU2E EXPERIMENT: A REVIEW

V.S. PRONSKIKH

Accelerator Physics Center, Fermi National Accelerator Laboratory,
MS 220, Kirk Rd and Pine Str, Batavia, IL 60510, USA
vspron@fnal.gov

Received (Day Month Year)
Revised (Day Month Year)

The Mu2e experiment being designed at Fermilab will be searching for a rare event – conversion of muon into electron the field of a nucleus without emission of neutrinos – observation of which would provide unambiguous evidence for physics beyond the Standard Model, making use of an 8 GeV 8 kW proton beam. As an experiment to be performed at the Fermilab's Intensity Frontier, taking advantage of high-intensity proton beams, Mu2e experimental setup will be residing in a harsh radiation environment, created by secondary particle fluxes.

Radiation quantities in different parts of the Mu2e apparatus, such as neutron flux, peak power density, DPA, absorbed dose, dynamic heat load simulated using the MARS15 code are reviewed in this work. Radiation levels and requirements for Heat and Radiation Shield (HRS), Transport Solenoid, residual dose and decay heat from the Mu2e target, beam dump design, rates in Cosmic Ray Veto counters as well as stopping target monitor are considered. Airflow, surface, and ground water activation are estimated. Recent developments in the MARS15 DPA model applied in this work are described, its consequences are discussed.

Keywords: muon to electron conversion; apparatus design; energy deposition; radiation damage; neutron background; Monte-Carlo simulations.

13.35.Bv; 07.05.Fb; 61.80.Hg; 28.20.Fc.

1. Introduction

The Mu2e experiment [1] at Fermilab is devoted to studies of the conversion of a negative muon to electron in the field of a nucleus without emission of neutrinos, as a result of the charged lepton flavor violation (CLFV). The emission of monoenergetic 105-MeV electrons can serve as a signature of such a process. This process has a very low probability ($< 10^{-54}$) in the Standard Model, however, it is predicted at the rates reachable by Mu2e by a number of theories beyond the Standard Model, such as SUSY theories, extra dimensions, leptoquarks, compositeness, second Higgs doublet etc. The Mu2e experiment is a further development of the previously proposed MECO [2] and MELC [3] experiments. Being an experiment

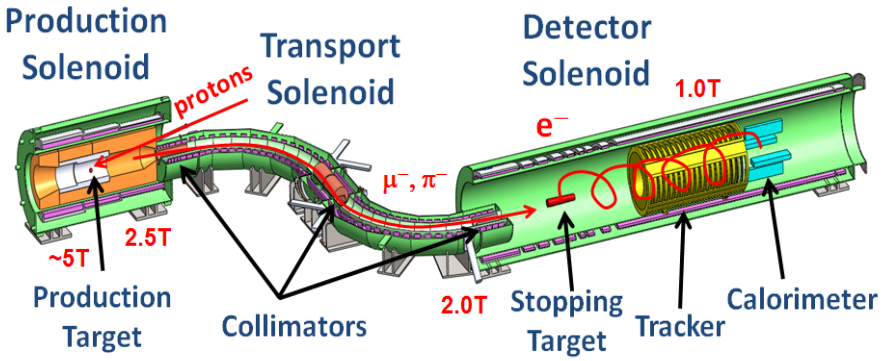

Fig. 1. Mu2e experimental setup model. (not shown: Cosmic Ray Veto, Proton Dump, Muon Dump, Proton/Neutron absorbers, Extinction Monitor, Stopping Monitor)

at Fermilab's Intensity Frontier, a branch of experimental research at Fermilab's high-intensity beams, Mu2e calls for very stringent requirements to shielding of the detector, environment, and such parts of apparatus as superconducting magnets. One of the main parts of the Mu2e experimental setup (see Fig. 1) is its superconducting production solenoid (PS), in which negative pions (later decaying into the target μ^- are generated among other secondaries in interactions of the primary proton beam with a target. The off-axis 8 GeV proton beam will deliver $6 \cdot 10^{12}$ protons per second to the tungsten target, placed at the center of the PS bore. In order for the PS superconducting magnet to operate reliably, the peak secondary neutron flux must be reduced down to acceptable levels by means of the proposed sophisticatedly designed Heat and Radiation Shield (HRS), optimized for the performance and cost.

Besides PS magnets, other critical parts of the Mu2e apparatus from the radiation shielding point of view are superconducting magnet coils, far upstream and middle transport solenoid (TS) coils, production target (its residual activation and decay heat), Cosmic Ray Veto counters (neutron background), stopping target monitor (STM) (photon background and radiation damage), and beam dump (its residual activation and power density) (see Fig. 1). Airflow in the PS hall, ground and surface water activation in the soil surrounding the PS hall are also important parameters of the environmental protection, which are also studied using MARS15 [5,4] code.

2. Requirements to PS Heat and Radiation Shield

HRS serves to protect the superconducting coils of the Production Solenoid (PS) from the intense radiation generated by the primary (8 kW) 8 GeV kinetic energy proton beam striking the production target within the warm bore of the PS. It also protects the coils in the far upstream end of the Transport Solenoid (TS), a straight section of coils (called TS1), at the exit from the PS. The HRS aperture should allow the maximum stopping rate of negative muons in the Detector Solenoid (DS) stopping target.

There is a number of requirements for the HRS [11]:

(1) Production Solenoid Heat and Radiation :
   - Limit the continuous power delivered to the cold mass.
   - Limit the local heat load allowed anywhere within the superconducting coils.
   - Limit the maximum local absorbed radiation dose to the superconductor insulation and epoxy over the lifetime of the experiment.
   - Limit the damage to the Al stabilizer of the superconductor.

(2) Production Solenoid field quality should not be degraded by materials used in the HRS.
(3) Production Solenoid forces during a quench should be minimized by the choice of HRS materials to the possible extent. The HRS electrical resistivity must be high enough to limit forces from eddy currents during a quench.
(4) Transport Solenoid Heat and Radiation (see 1 above).
(5) HRS Thermal Cooling.
(6) The HRS must also be adaptable to the design of a remote handling system for the pion production target.
(7) Muon yield should not be reduced significantly by the inner bore size of the HRS.
(8) Shield design must avoid any line-of-sight cracks between components that point from the target to the inner cryostat wall and thus the magnet coils.

2.1. *Peak power density limit*

Peak power density is limited by the requirement to the instantaneous local heat load allowed anywhere within the superconducting coils. The 3D thermal analysis was performed for the radiation heat load in case of the optimized absorber design [15]. The FEM model created by the magnet group using COMSOL Multiphysics was discretized to the level of individual layers and the interlayer insulation/conducting sheets. The thermal conductivities of individual layers in the axial direction were substituted by the equivalent thermal conductivity of the insulated cable.

The dynamic heat load map in the coil and the support structure generated by the MARS15 code was applied to all parts of the cold mass. The maximum temperature is in the middle of the inner surface of the thickest coil section; that

location coincides with the peak field location, and, therefore directly affects the thermal margin. On the basis of the thermal analysis, limit to peak power density in the Al coil structures was found to be 30 μW/g. Nevertheless, that limit is used only for preliminary estimation during HRS optimization steps, while for detailed analyses temperature distribution and rise based on the entire heat map is studied.

2.2. *Displacements per atom (DPA) damage*

Radiation damage to the atomic lattice of a superconducting cable, and its quench stabilizing matrix made from normal conductor takes the form of the accumulation of such lattice defects as atomic displacements (formation of pairs of vacancies and interstitial atoms as well as defect clusters). Damage to a metal sample exposed to a flux of penetrating particles can be characterized by the average number of displacements per atom (DPA). The DPA damage effect is directly related to electron transport in metals, leading to Residual Resistivity Ratio (RRR) degradation. RRR is defined as the ratio of the electrical resistance at room temperature of a conductor to that at 4.5 K, which decreases after an irradiation.However, warming such a sample to room temperature (annealing) leads to recovery of the RRR [24], but the degree of recovery is different for metals with different crystalline latices. Aluminum is a material that shows complete recovery at 300 K. The annealing time has a time scale of minutes [16]. This time scale needs to be compared to cryogenic heat capacity as well as expected thermal stresses for the PS during warm-up or cool-down cycles, which can take days.

2.3. *The effect of RRR on the magnet performance*

RRR affects the magnet performance during operation in superconducting mode and its transition to the normal state (also called quench). Magnet stability is the ability of coils to recover the superconducting state after a short time-scale transition into the normal state without the quench. The superconductor transition to the normal state occurs when either the magnetic field, temperature or current exceed the critical values. When quenches, the electric current in the superconductor is removed into the surrounding Cu and Al stabilizers that have much lower resistivity than the superconductor in its normal conductor state. If the stabilizer resistivity is low enough (that corresponds to a high RRR), the temperature can return to the operating temperature after an excursion. Otherwise, the normal conductivity zone can propagate and eventually transit to the normal state entirely, i.e. quench. (for more discussion of the quench mechanisms see also Chapter 7 in [1]).

The final magnet design will be optimized to work at the minimum RRR of 100 for aluminum and 50 for copper set forth in the PS requirements Requirements document Document [11] with sufficient operating margins. However, these margins, governed by the practices applicable to the design of superconducting magnets, however, do not account for the errors in determining DPA and RRR. Therefore, it is important that the HRS design requirement includes an appropriate safety

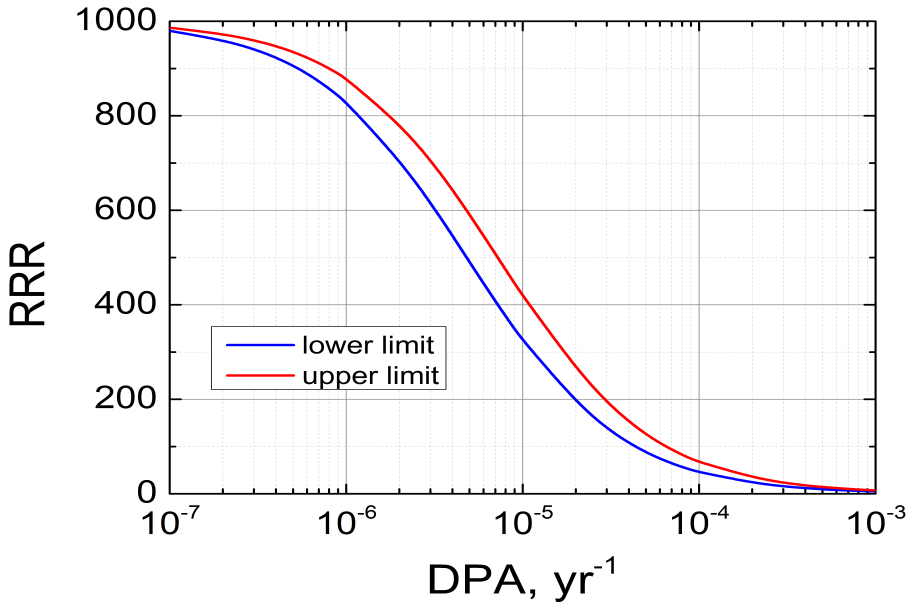

Fig. 2. RRR as a function of DPA for Al.

margin in the maximum acceptable value of DPA to account for these errors, in order to guarantee meeting the minimum RRR requirements with a 5% accuracy.

Dependence of RRR on DPA, having the form $RRR = \frac{\rho_{hi}}{\rho_0 + \Delta\rho(DPA)}$, is presented in Figure 2. Al resistivity at high temperature ρ_{hi} was taken to be $2.7 \cdot 10^{-7} \Omega * cm$, its resistivity at the cryogenic temperatures is required to be $\rho_0 = \frac{\rho_{hi}}{1000}$. Value of resistivity degradation per DPA $\Delta\rho$ was determined from recent KEK measurements [23] with an Al stabilizer sample exposed to a reactor neutron spectrum at low temperatures. DPA rates were calculated using MARS15 DPA model, based on FermiDPA 1.0 library, which includes also a correction for the defect production efficiency η, as described in the section 2.4. Due to a 15% uncertainty in η value, RRR shown in Figure 2, is represented by two curves, reflecting that uncertainty. Applying the requirement of RRR degradation from 1000 to 100, we determine the limit on DPA to be $4 \div 6 \cdot 10^{-5}$ yr^{-1}.

2.4. *DPA damage and its modeling in MARS15*

The atomic displacement (DPA) model was recently refined in MARS15 and verified against data and other theoretical models. DPA is now reliably calculated from 1 keV to several TeV for charged particles and heavy ions, and from 0.001 eV up for neutrons. The MARS15 version used employs the model of displacements, produced by elastic Coulomb scattering of charged particles improved by modification of the screening parameter. Range of applicability of the current model has been recently significantly increased, especially for low-energy heavy particles [17].

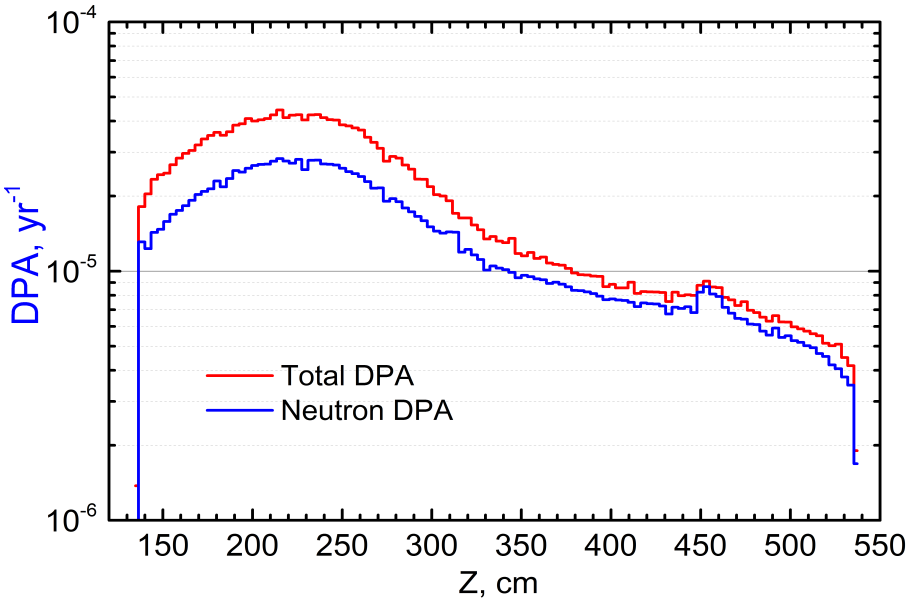

Fig. 3. Contribution of the neutron component to DPA at the HRS hot spot. Horizontal axis corresponds to that in Fig. 6

.

A new model was recently developed for neutrons from 10^{-5} eV to 20-150 MeV using the ENDFB-VII [12] database for 393 nuclides. This model implementation in MARS15 code is based on the application of FermiDPA 1.0 cross section library (see Fig. 5), which was calculated using NRT [9] model as implemented in NJOY [10] code for all nuclides covered by ENDFB-VII ($N_{NRT} = \frac{0.8}{2 \cdot E_d} \cdot T_{dam}$, E_d – threshould energy, T_{dam} – damage energy). In the current MARS15 implementation FermiDPA 1.0 cross sections are used at neutron energies below 14.5 MeV. For materials at low temperatures ($\leq$ 4.2 K), like the superconducting magnet coil material, the NRT DPA rates are corrected using experimental defect production efficiency η, which is a ratio of a number of single interstitial atom vacancy pairs (Frenkel pairs) produced in a material to the number of defects calculated using NRT model ($\eta = N_d/N_{NRT}$). The values of η have been measured experimentally [8] for many important materials for a number of neutron spectra in the reactor energy range (below 14.5 MeV). Scaling the DPA rate obtained using NRT model to the experimental ones using η leads to a decrease of the resulting one by a factor of 2 – 3 (see Fig. 4) on average , because in the case of HRS "hot spot" on coils, which is near the spent beam exit close to the middle of the first coil (see Fig. 6), more than 99% of neutrons have energies below 14.5 MeV. For the HRS coils neutrons contribute to the total DPA about 70% (see Fig. 3). This explains significant (up to 40%) growth of DPA levels when the new DPA model was used instead of the old one.

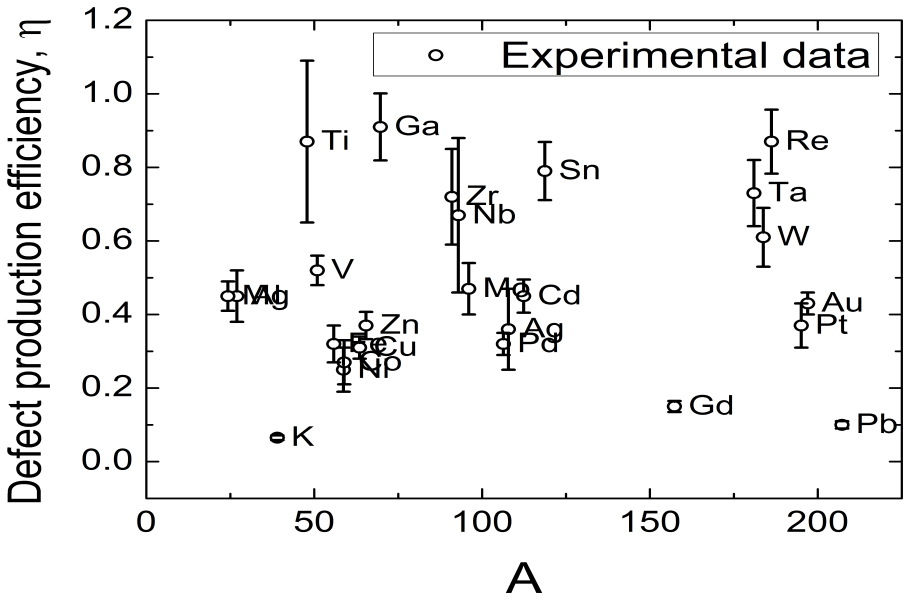

Fig. 4. Experimental defect production efficiencies used by MARS15.

2.5. *Absorbed dose to organic materials*

This quantity limits the maximum local absorbed radiation dose to the superconductor insulation and epoxy over the lifetime of the experiment. In principle, each material included in the construction of the magnet should be rated for the maximum allowable local radiation dose over the operational lifetime. In practice, the most radiation sensitive material sets the lower limit; in particular, the epoxy used to bond the insulation to the superconducting cable can tolerate a maximum of 1 MGy before it experiences a 10% degradation in its shear modulus and the insulation may absorb 350 – 400 kGy/yr [18].

2.6. *Dynamic heat load*

Limit to the dynamic heat load as the continuous power delivered to the cold mass is related to the number of cooling stations the experiment will be using. An acceptable shield design should establish the following quench limits for nominal operating conditions with the proton beam hitting the target: the maximum allowable total heat load for the PS coils is 100 W [22]; this is a conservative value given that the design of the cryogenic system for the PS is still in progress.

2.7. *Current Mu2e limits*

Limits on the radiation quantities [11] thus were set based on: quench protection requiring that peak coil temperature does not violate allowable value of 5 K with

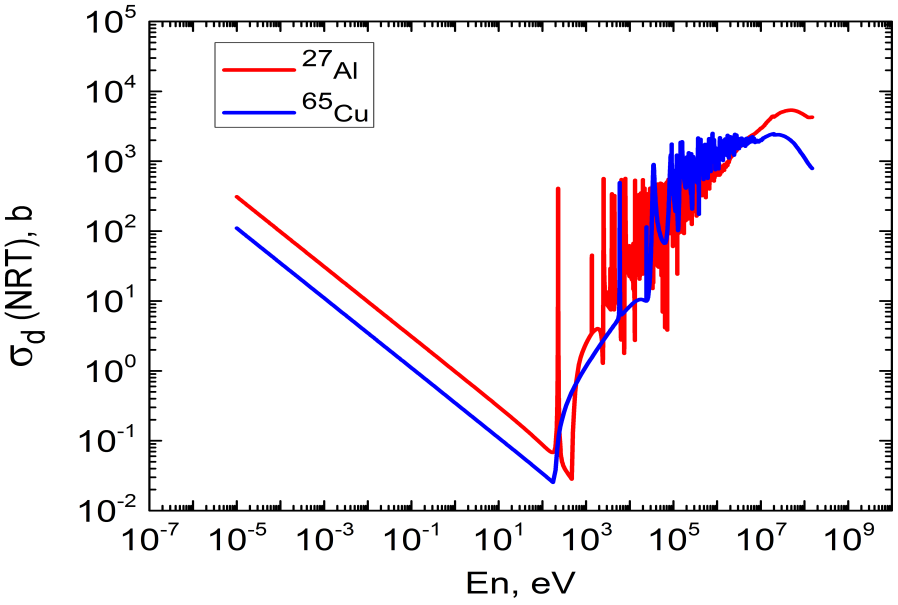

Fig. 5. DPA cross sections for Al and Cu from FermiDPA 1.0 library

1.5 K thermal margin for peak power density, 10% degradation of ultimate tensile strength for absorbed dose, RRR (residual resistivity ratio) degradation from 1000 to 100 in Al stabilizer, and requirements from the particular cooling system designed for dynamic heat load. In the current design peak power density is limited to 30 μW/g, peak DPA – $4 \div 6 \cdot 10^{-5}$, peak absorbed dose over the experiment lifetime – 7 MGy, and dynamic heat load – 100 W.

3. Mu2e MARS15 simulated design levels

Simulations of the design levels have been performed using MARS15 code with 0.001 eV thresholds for neutrons (MCNP mode using ENDFB-VI library), 200 keV for γ-quanta, and 100 keV for charged hadrons. To describe the interactions of particles above few MeV the exclusive hadron-nucleus model employing LAQGSM [6] model above 3 GeV, and CEM [7] below was used. Proton beam intensity was $6 \cdot 10^{12}$ p/s, which corresponds to 8 kW. PS was surrounded by a 0.5 m thick concrete shield, which partly reflects neutrons. Spectra of neutrons and photons are shown in Fig. 7. Baseline for the initial stages of Mu2e project was the model given in Fig. 6. Spectra show that the initially spallation spectrum produced by protons on the tungsten target and high-energy secondary hadrons in the innermost parts of the HRS inner bore are then essentially slowed down by bronze when reach the coils. The flux of photons is comparable to that of neutrons at 10 MeV, however their contribution to the radiation damage is significantly less. Bronze used in the HRS model has the density of 7.64 g/cm^3. PS coil material contains 64% of Al, 11.5% of NbTi, and

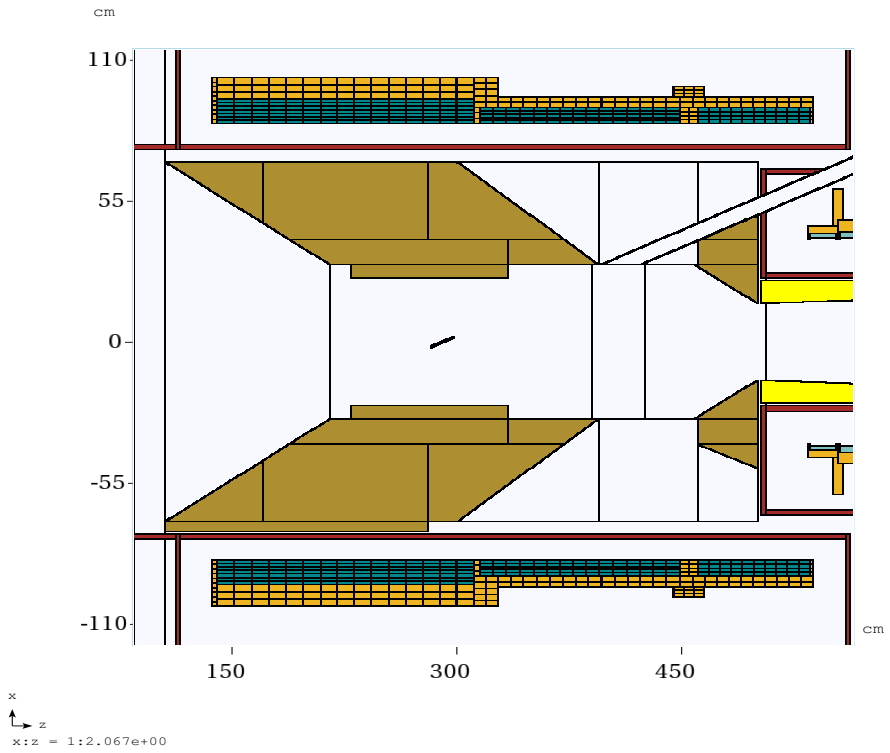

Fig. 6. MARS15 Mu2e PS model. Parts are: brown – Heat and Radiation Shield (bronze), green – NbTi/Al superconducting coils, orange – Al support structure, gray – concrete shield, yellow – Cu collimator leading to the muon transport system.

10.4% of copper (in the simulations the homogeneous mix is used).

3.1. *Power density*

Besides the peak power density, shown in Fig. 8 (red line, right scale), heat maps for the thermal analysis are always produced in the course of simulations. Thermal maps help determine temperature rise in coils for particular cooling schemes and simulate the quench propagation conditions. The figure shows that the peak power density in the coils is 17μW/g, which is well below the critical 30μW/g, however, the heat map analysis can impose additional constrains on design. Power density drops from the peak down by more than an order of magnitude thus suggesting a reduction of material upstream the target in the vicinity of the second and third coils. However, such a reduction requires further thermal analysis of trade-off with the quench propagation in the coils, which is affected by not only the peak value of the power density, but also its 3D distribution in the entire cold mass.

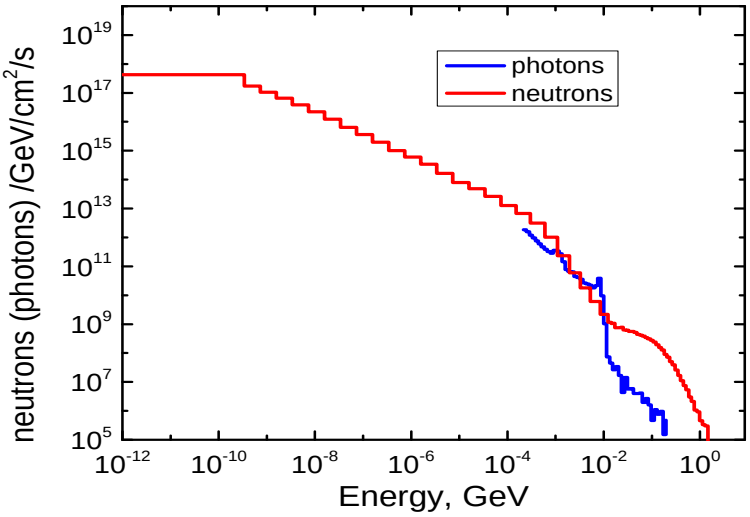

Fig. 7. Neutron and photon spectra in the first PS coil.

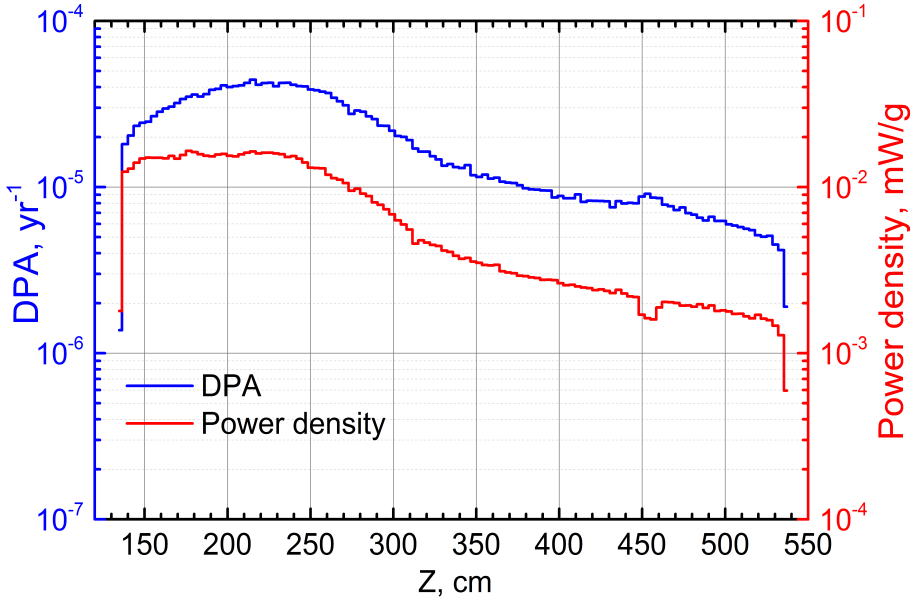

Fig. 8. Displacement per atom and power density levels in PS superconducting coils.

3.2. *DPA*

DPA distribution in the coil strip near the beam exit (under the same assumptions as for the peak power density) is shown in Fig. 8 (blue line, left scale). The peak

DPA rate, which is about $4.4{\cdot}10^{-5}$ yr^{-1}, corresponds to approximately the first third of the first coil, and then falls off in the upstream direction (along Z axis) by the same factor as in the case of the power density.

3.3. *Absorbed dose*

Distribution of the absorbed dose in the hottest strip of the HRS magnet coils and structures resembles that of the power density shown in Fig. 8, however, requires a unit conversion from mW/g to Gy/s. For $2 \cdot 10^7$ s, representing a working year for fixed target experiments, such scaling gives 340 Gy/yr for 17 μW/g as the peak absorbed dose. Assuming the lifetime of the Mu2e experiment to be 5 years, we obtain the design value of 1.7 MGy, which is under the limit of 7 MGy with a good safety margin.

3.4. *Accidental mode levels*

The simplest accidental mode modeled is the beam mis-steering at the upstream edge of the HRS near the beam pipe entrance location (see Fig. 9). Peak values attained in such a mode are $1 \cdot 10^{-14}$ DPA (per 1 ms, which was assumed to be a characteristic time scale for an accidental mode), peak energy deposition – 0.1 μJ/g for the same time. These values are considered to be far from the potentially dangerous levels. Similar simulations performed for the beam mis-steered within the beam pipe near the TS1 coils showed that in the case of such kind of accidental mode the coils are still safe within that time scale.

4. Residual activation of Production Solenoid coils

Residual dose simulations for production solenoid parts show that the dose on contact with PS coils and Al stabilizer will be ~ 0.7 mSv/hr after a year of irradiation and a week of cooling, and ~ 80 μSv/hr after 30 days of irradiation and a week of cooling, which is rather high and requires particular safety measures for personnel performing PS maintenance during the lifetime of the experiment.

5. Radiation quantities at Transport Solenoid

Transport Solenoid coils are endangered by the secondaries produced in the production target and PS HRS as well as by those created by pions and muons in both the far upstream and middle TS collimators. The far upstream TS1 collimator is designed from copper with the inner carbon layer (to suppress $\bar{p}$ production), and the entire middle TS collimator is from copper. Far upstream TS1 coils have the following composition : 8.27% of NbTi alloy, 9.51% of Cu, 15.53% of G10, 66.69% of Al, its stabilizer structure is made of Al 5083. Peak values obtained for TS1 coils by MARS15 simulations are power densities : $1.7 \cdot 10^{-3}$ mW/g for coils and $1.4 \cdot 10^{-3}$ mW/g, DPA : $\sim 1 \cdot 10^{-5}$ yr^{-1}, absorbed dose : 23 kGy/yr. Total dynamic heat load in TS1 is 0.25 W.

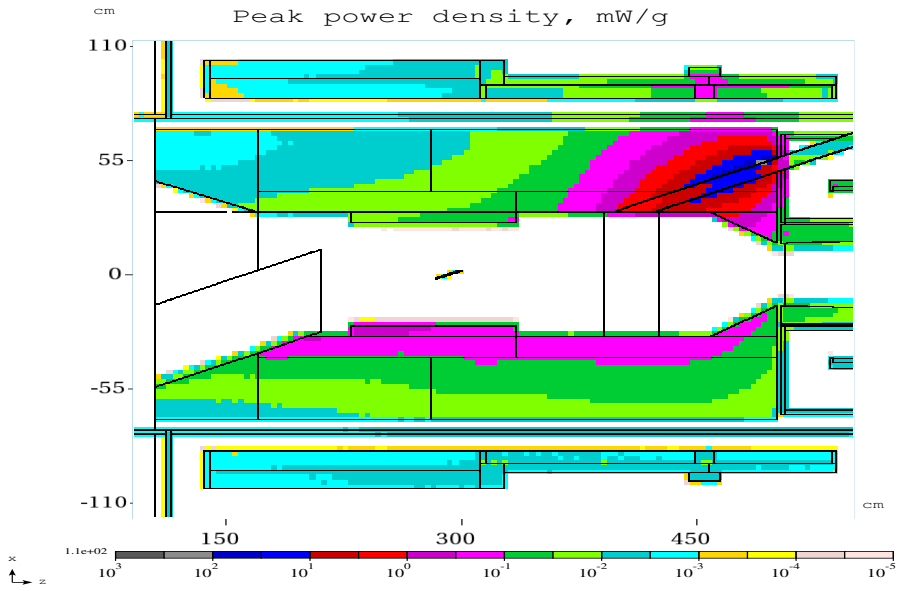

Fig. 9. Power density in an accidental mode beam on HRS.

Middle collimator TS3 coils have the following composition : bobbins and flanges : Si 0.4%, Fe 0.4%, Cu 0.1%, Mn 0.4%, Mg 4%, Zn 0.25%,Ti 0.15%, Cr 0.05%, Al 94.25% (Al 5083), coils : NbTi 8.27%, Cu 9.51%, G10 15.53%, Al 66.69%. Additional source of neutrons near TS3 are pions and muons (especially positively charges, which are filtered out by the middle collimator). Peak DPA at the TS3 coils is at the level of $1 \cdot 10^{-6}$ yr^{-1}, power density – $0.5 \cdot 10^{-3}$ mW/g, absorbed dose – 10 kGy/yr. Total dynamic heat load in the middle collimator is $\sim$ 21 W.

6. Production target

Mu2e baseline production target is a tungsten cylinder with the radius of 3.15 mm. For Mu2e at 25 W beam, a gold target was previously considered, and MARS15 simulations gave for that option the residual dose on contact of 20 kSv/hr (see Fig. 11). Methods were developed and applied to scale that dose to that at various distances [21], and it was shown that the dose reduces down to $\sim$ 13 Sv/hr at the distance of 30 cm, and down to 1.5 Sv/hr at 100 cm. This reduction is very significant due to small dimensions of the target, and allow to apply regular shielding measures in the course of the experiment. Correction to the current 8 kW baseline beam power also reduces the dose by another factor of 3.

Decay heat calculations have been done using a combination of MARS15 and DeTra code [19], in order to estimate contribution from the decay heat to the energy release in the target and how it affects the cooling requirements. It was demonstrated that out of $\sim$ 1400 nuclides, produced in the target by the primary beam,

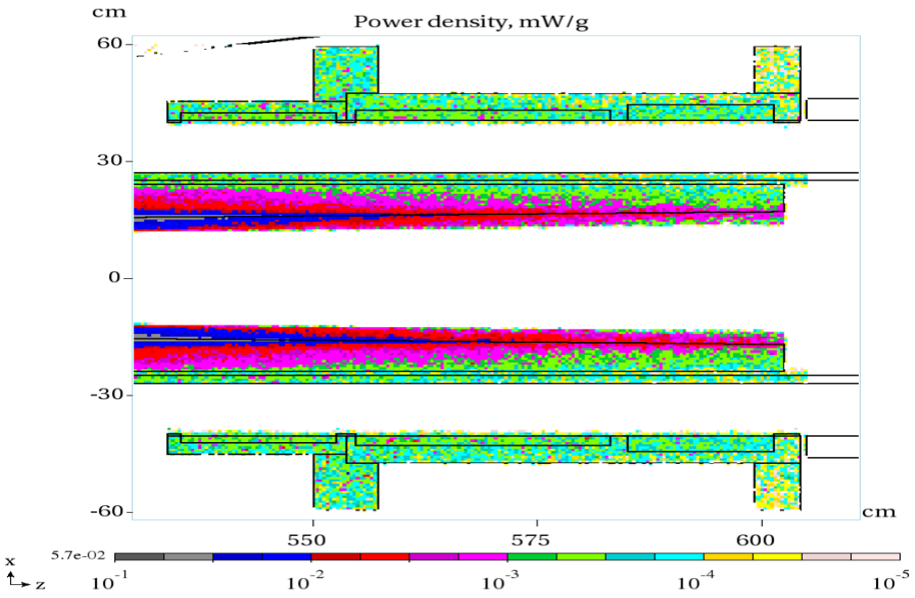

Fig. 10. Power density distribution in the TS1 collimator coils.

31 contribute more than 1% each to the decay heat (60% of the total all of them), and the rest contributes the other 40%. Finally, decay heat amounts to 11.3 W when beam is on, and rapidly falls off (down to below 1 W over a week) after it is off. Contribution of the decay heat to the total power release in the target is shown to be negligible relatively to the dynamic heat load by the primary beam (∼800 W at 25 kW). To scale the numbers down to the current 8 kW baseline beam power the same factor of 3 applies. It is not expected that transition from a gold to a tungsten target will affect the numbers significantly due to the close mass numbers and densities of the metals.

7. Beam dump

Beam dump is a 1.5x1.5x2 m box of either Al or steel, surrounded by concrete. Simulations were made for both materials, steel being the latest option under consideration due to its relatively low cost. Heat map of the beam dump options are analysed in order to find the most appropriate cooling scheme, peak power density, for instance, for the Fe option being 1.9 mW/g for the working mode. Power, released in the steel dump as determined by MARS15 simulations is 1.3 kW, subsequent ANSYS analysis gives 44.5°C for the core temperature, and 25.8°C for the surrounding concrete. Under all the thermal conduction scenarios, the peak temperature is below the critical 100°C, thus the analysis shows the feasibility of the steel dump option.

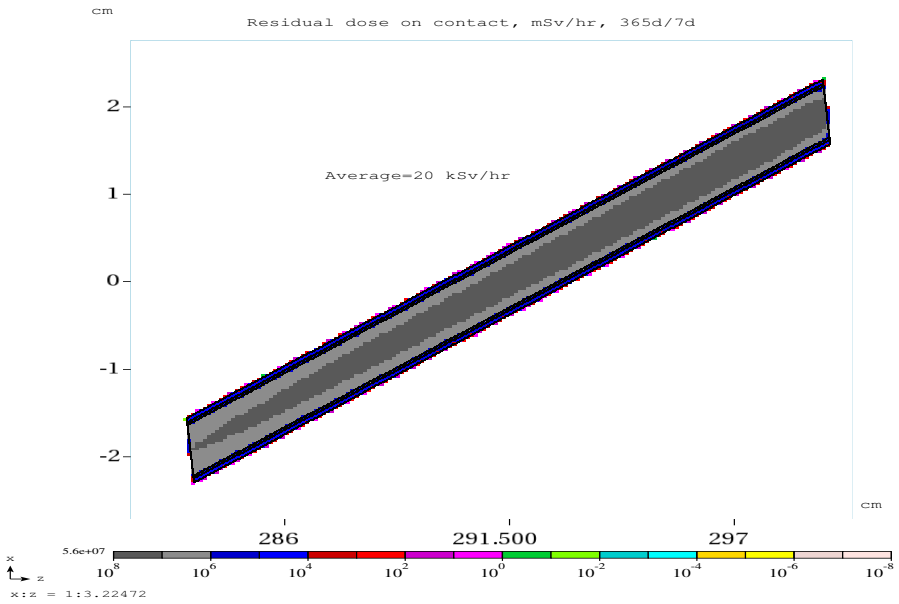

Fig. 11. Residual dose on target.

7.1. *Airflow activation*

For the air activation estimations, the entire PS hall volume was subdivided in 16000 boxes with the dimensions 1x1x3x feet, and maps for the distribution of radiation quantities is obtained. Peak power density in the air is 6.4 mW/g, peak neutron flux – $2.6 \cdot 10^9$ n/cm^2/s, peak photon flux – $1.1 \cdot 10^{10}$ 1/cm^2/s. Peak gases production in the hall was found to be $2.7 \cdot 10^5$ at/cm^3/s for hydrogen, $2.1 \cdot 10^4$ at/cm^3/s for helium, and $2.0 \cdot 10^3$ at/cm^2/s for tritium. The detailed analysis of these maps is ongoing.

Air activation and flow estimations show that at 500 cfm, for the configuration without a pipe connecting the target region to the beam dump (average hadron flux over the whole hall volume is $5.5 \cdot 10^6$ cm^{-2}s^{-1}), the maximum annual activity released from the target hall is less than 29 Ci, which is $\sim 7\%$ of the Labs air release limit.

7.2. *Surface and ground water activation*

Based on MARS15 simulations of the hadron flux and star density and using the Fermilab standard Concentration Model [20] at the design intensity, the average concentrations of radionuclides in the sump pump discharge were calculated as 24 pCi/ml due to ^{3}H and 2 pCi/ml due to ^{22}Na. This is 2% of the total surface water limit if the pumping is performed once a month (conservative scenario). Build-up of these nuclides in ground water at $1.2 \cdot 10^{20}$ protons per year will be as low as

$6.2 \cdot 10^{-8}$ % of the total limit over 3 years of operation.

8. Radiation damage and noise in Cosmic Ray Veto counters

MARS15 simulations showed that the neutron flux in Cosmic Ray Veto (CRV) counters, surrounding the Detector Solenoid, significantly violates the limit of 10^{10} n/cm^2/s, critical for the radiation damage in Silicon Photomultipliers (SiPM) at certain "hot spots". Another effect critical for CRV electronics performance is the noise, created by a high neutron rate. The neutrons, contributing to the flux levels, originate from such sources as the PS (production target and HRS), beam line (TS collimators), stopping target, and the muon beam stop. Simulations are under way to find solutions capable of mitigating the effect of the background neutrons on CRV counters and improve shielding around them. SiPm irradiation experiments are being planned to determine the limit more precisely.

9. Stopping target monitor radiation damage

The stopping target monitor (STM) is a Ge crystal detector which will be installed at the downstream end of the Detector Solenoid, and will be counting X-rays of the muonic atoms formed in the stopping target in the course of the experiment. High neutron flux to the STM can lead to the DPA damage of the crystal, and subsequent detector resolution degradation [14]. Peak DPA rate, simulated by MARS15 code was found to be $\sim 10^{-8}$ yr^{-1}, and neutrons flux ~ 5600 n/cm^{-2}s^{-1}, almost all neutrons having energies above 100 keV. It was estimated that for an n-type HPGe detector, average peak FWTM will increase by 25% in $\sim$5 days. It is suggested that a study of resolution degradation per neutron flux needs to be done for the particular detector type to be used in the experiment. Flux of γ-quanta has also been determined at the level of $3.4 \cdot 10^4$ 1/cm^2/s, and a γ energy spectrum was simulated, because of their ability to create the continuous background in the detector during measurements and thus contribute the uncertainty of the result.

10. Conclusion

Present state-of-the-art of radiation studies that are carried out in the course of the design and simulation studies of the Mu2e experimental setup have been reviewed. Requirements to the levels of radiation quantities as well as their grounds have been discussed. Working and partly accidental mode levels for Heat and Radiation Shield, Transport Solenoid, production target, beam dump, Cosmic Ray Veto counters, and Stopping Target Monitor, as well as airflow, surface and ground water activation are estimated. Further work directions on HRS, CRV, and STM, which are underway, are suggested.

The author is indebted to Drs. R. Ray, R. Bernstein, and J. Miller for the organization and coordination of the efforts on the design of the Mu2e experiment, Drs.

M. Lamm, V.V. Kashikhin, G. Ambrosio, J. Popp, R. Coleman for their conclusive contribution at all stages of magnet, HRS, target systems design. The author is thankful to Drs. N.V. Mokhov and R. Coleman for reading the manuscript and many useful discussions during his work on this review and beyond.

References

1. R.J. Abrams *et al.*, Mu2e Conceptual Design Report Fermilab-TM-2545, (2012).
2. M. Bachman *et al.*, research proposal to Brookhaven National Laboratory, 1997.
3. R. Djilkibaev and V. M. Lobashev, Sov. J. Nucl. Phys. **49(2)**, 384 (1989).
4. N.V. Mokhov *et al.*, Technical Report FERMILAB-CONF-12-635-APC, 2012.
5. N.V. Mokhov *et al.*, Fermilab Report Fermilab-FN-628 (1995); N.V. Mokhov *et al.*, AIP Conf. Proc. 896, pp. 50-60 (2007); http://www-ap.fnal.gov/MARS/.
6. S.G. Mashnik *et al.*, LANL Report LA-UR-08-2931, (2008); arXiv:0805.0751 v1 [nucl-th] 6 May 2008.
7. S. G. Mashnik *et al.*, LANL Technical Report LA-UR-05-7321, (2005).
8. C.H.M. Broeders, A.Yu. Konobeev, Journal of Nuclear Materials, **328**, 197 (2004).
9. M.J. Norgett *et al.*, Nuclear Engineering and Design, **33**, 50 (1975).
10. R. E. MacFarlane *et al.*, LANL Preprint LA-12740-M, (1994).
11. G. Ambrosio *et al.*, Fermilab Report Fermilab-FN-0954-AD-APC-TD (2013).
12. M.B. Chadwick *et al.*, Nuclear Data Sheets **107**, 2931 (2006).
13. V.S. Pronskikh *et al.*, Fermilab-FN-0930-APC (2011).
14. V.Borrel *et al.*, NIM A **430**, 348 (1999).
15. V.S. Pronskikh *at al.* Proceedings of 2011 Particle Accelerator Conference, New York, NY, USA, **THP048**, (2011).
16. J. A. Horak and T. H. Blewitt, J. Nucl. Mat., **49**, 161 (1973/74).
17. N.V. Mokhov *at al.*, accepted to Progr. Nucl. Sci. Tech., (2013).
18. N.J. Simon, Technical Report NISTIR-3999, 51 (1993).
19. P. Aarnio, Technical Report CMS-NOTE-1998/086, CERN, (1998).
20. A.J. Malensek et al, Fermilab-TM-1851, (1993).
21. V.S. Pronskikh *et al.* Fermilab-FN-0930-APC, 2011.
22. Ref. [1], 5-91.
23. M. Yoshida *et al.*, Proceedings of IPAC2012, New Orleans, Louisiana, USA, **THPPD024**, (2012).
24. M.Guinan *et al.*, J. Nucl. Mater., **133&134**, 357 (1985).